Pixel based fusion using IKONOS imagery

Uttam Kumar, Chiranjit Mukhopadhyay, and T. V. Ramachandra*
Indian Institute of Science, Bangalore, India.
Email: uttam@ces.iisc.ernet.in, cm@mgmt.iisc.ernet.in, cestvr@ces.iisc.ernet.in

***Abstract*— Pixel based image fusion entails combining geometric details of a high-resolution Panchromatic (PAN) image and spectral information of a low-resolution Multispectral (MS) image to produce images with highest spatial content while preserving the spectral information. This work reviews and implements six fusion techniques – À Trous algorithm based wavelet transform (ATW), Mulitresolution Analysis based Intensity Modulation, Gram Schmidt fusion, CN Spectral, Luminance Chrominance and High pass fusion (HPF) on IKONOS imagery having 1 m PAN and 4 m MS channels. Comparative performance analysis of techniques by various methods reveals that ATW followed by HPF perform best among all the techniques.**

***Index Terms*— Image merging, multispectral, resolution**

I. INTRODUCTION

Most Earth observational satellites are not capable of providing high spatial and spectral resolution data simultaneously because of design or observational constraints. To overcome such limitations, image fusion (also called *pansharpening*) techniques are used to integrate the high resolution (HR) Panchromatic (PAN) and low resolution (LR) multispectral (MS) bands that exhibit complementary characteristics of spatial and spectral details for image analysis and automated tasks such as feature extraction, segmentation, classification, etc. The standard merging methods are based on the following steps: (i) Registration of the LR MS image to the same size as the HR PAN image in order to be superimposed. Usually, the images are registered up to within 0.25 pixels, resampling the MS using control points using a nearest neighbour or bi-cubic polynomial fit, (ii) Transformation of the LR MS bands to other space using any standard technique (such as PCA, Correspondence analysis, RGB to IHS, Wavelet, etc.), (iii) Replacement of the first component of the transformed LR MS image by the HR PAN image, (iv) Inverse transformation to get back the original MS images with high spatial and spectral resolutions. In many fusion techniques (such as High pass filtering, High pass modulation) instead of performing steps (ii), (iii) and (iv), the HR PAN image is convolved with a user designed filter and the resultant image is added to the LR MS image to obtain the HR MS image. In this communication, we implement six image fusion techniques – À Trous algorithm based wavelet transform, Mulitresolution Analysis based Intensity Modulation, Gram Schmidt fusion, CN Spectral, Luminance Chrominance and High pass fusion.

*Corresponding author: Energy Research Group, Centre for Ecological Sciences, Indian Institute of Science, Bangalore – 560012, India. Phone: 91-80-22933099; Fax: 91-80-23600683.

II. IMAGE FUSION METHODS

A. À Trous algorithm based wavelet transform (ATW): Multiresolution analysis based on the wavelet transformation (WT) is based on the decomposition of the image into multiple channels depending on their local frequency content. While the Fourier transform gives an idea of the frequency content in image, the wavelet representation is an intermediate representation and provides a good localisation in both frequency and space domain [1]. The WT of a p.d.f. (probability density function) *f(t)* is expressed as

$$W(\mathrm{f})\,(a,b) = |a|^{-\frac{1}{2}} \int_{-\infty}^{+\infty} f(t)\psi\left(\frac{t-b}{a}\right)dt \qquad (1)$$

where a and b are scaling and transitional parameters, respectively. Each base function $\psi\left(\frac{t-b}{a}\right)dt$ is a scaled and translated version of a function ψ called *Mother Wavelet*. These base functions are such that $\int_{-\infty}^{\infty}\psi\left(\frac{t-b}{a}\right)\mathrm{d}t = 0$. Most of the WT algorithms produce results that are not shift invariant. An algorithm proposed by Starck and Murtagh [2] uses a WT known as à trous to decompose the image into wavelet planes that overcomes this problem. Given an image $\mathbf{p}$ we construct the sequence of approximations: $F_1(\mathbf{p}) = \mathbf{p}_1$, $F_2(\mathbf{p}_1) = \mathbf{p}_2$, $F_3(\mathbf{p}_2) = \mathbf{p}_3$, ... by performing successive convolutions with a filter obtained from an auxiliary function (F_1, F_2, F_3) named scaling function which has a $\mathbf{B_3}$ cubic spline profile. The use of a $\mathbf{B_3}$ cubic spline leads to a convolution with a mask of 5 x 5:

$$\frac{1}{256}\begin{pmatrix} 1 & 4 & 6 & 4 & 1 \\ 4 & 16 & 24 & 16 & 4 \\ 6 & 24 & 36 & 24 & 6 \\ 4 & 16 & 24 & 16 & 4 \\ 1 & 4 & 6 & 4 & 1 \end{pmatrix}. \qquad (2)$$

The wavelet planes are computed as the differences between two consecutive approximations $\mathbf{p}_{l-1}$ and $\mathbf{p}_l$. Letting $\mathrm{w}_l = \mathbf{p}_{l-1} - \mathbf{p}_l$ ($l = 1, \ldots, n$), in which $\mathbf{p}_0 = \mathbf{p}$, the reconstruction formula can be written as

$$\mathrm{p} = \sum_{l=1}^{n} w_l + \mathrm{p}_\mathrm{r}. \qquad (3)$$

The image $\mathbf{p}_l$ ($l = 0, \ldots, n$) are versions of original image $\mathbf{p}$, $\mathbf{w}_l$ ($l = 1, \ldots, n$) are the multiresolution wavelet planes, and $\mathbf{p}_r$ is a residual image. The wavelet merger method is

based on the fact that, in the wavelet decomposition, the images $\mathbf{p}_l$ (l = 0, …, n) are the successive versions of the original image. Thus the first wavelet planes of the HR PAN image have spatial information that is not present in the MS image. In this paper, we follow the Additive methods [1] where the HR PAN image is decomposed to n wavelet planes. For 1:4 fusion (as in IKONOS image) n is set to 2.

$$\mathbf{PAN} = \sum_{l=1}^{n} w_{\mathrm{P}l} + \mathbf{PAN}_r \quad (4)$$

The wavelet planes (W_{Pl}) of the PAN decomposition are added to the LR MS images individually to get HR MS images.

B. Multiresolution Analysis–Based Intensity Modulation (MRAIM): MRAIM [3] takes into consideration M-band wavelet theory [4] and à trous algorithm [5]. Multiresolution analysis decomposition method is the tool to decompose signals to their approximation and detail information. M-band wavelet is different from the most popularly used dyadic WT in the sense that M-band WT decomposes the frequency domain into M-channels while dyadic WT decomposes into 2 channels. So M-band WT can be used to compute the approximations at resolution M (M is an arbitrary integer larger than 0) while dyadic WT is limited to the resolution of 2^r (r ε I). The key problem to realise this approach is to construct K-regularity M-band scale filters (the construction of K-regularity M-band scale filters is explained in more detail at http://www.ee.umanitoba.ca/~ferens/wavelets.html). K-regularity is equivalent to saying that all polynomials of degree (K-1) are contained in approximation. This coupled with the compact support characteristic of the scaling filters implies that K-regularity scaling filters can be used to capture local polynomial behaviour. Steffen et al., (1993) [4] introduced the formula for K-regularity M-band scaling filter $H_0(z)$ in the Z transform of the analysis and synthesis process of the M-band scaling, which is just as in the 2-band case Daubechies' construction. For K=2, the minimal phase solution for arbitrary M is

$$Ho(\mathrm{z}) = \left[\frac{1+\mathrm{z}^{-1}+\ldots+z^{-(M-1)}}{M}\right]^2 (q_{(0)} + q_{(1)} z^{-1}) \quad (5)$$

where,

$$q_{(0)} = \frac{\sqrt{M}}{2}\left[1 \pm \sqrt{\frac{2M^2+1}{3}}\right] \text{ and } q_{(1)} = \frac{\sqrt{M}}{2}\left[1 \pm \sqrt{\frac{2M^2+1}{3}}\right] . \quad (6)$$

Upon the construction of the scale filters, the à trous algorithm is applied to compute the PAN image at the LR level by filtering. Given an image $\mathbf{p}_1$, at resolution level 1, the approximation $\mathbf{p}_M$ at resolution level M can be computed by low-pass filtering the image $\mathbf{p}_1$. The reconstruction formula is $\mathbf{p}_1 = \mathbf{p}_M + \mathrm{w}$ (7)

Once the approximation image $\mathbf{p}_M$ is obtained, it can be used to estimate LR PAN ($\mathrm{DN}^{l}_{\mathrm{PAN}}$) and the HR MS ($\mathrm{DN}^{h}_{\mathrm{MS}}$) images as follows:

$$\mathrm{DN}^{h}_{\mathrm{MS}} = \mathrm{DN}^{l}_{\mathrm{MS}} + (\mathrm{DN}^{h}_{\mathrm{PAN}} - \mathrm{DN}^{l}_{\mathrm{PAN}}) \frac{\mathrm{DN}^{l}_{\mathrm{MS}}}{\mathrm{DN}^{l}_{\mathrm{PAN}}} \quad (8)$$

C. Gram Schmidt (GS) Fusion: In GS fusion [6] method, PAN band is simulated from the LR MS bands. A GS transformation is performed on the simulated PAN and the MS bands, where the simulated PAN band is employed as the first band. Then the HR PAN band is swapped with the first GS band. Finally, the inverse GS transform is applied to form the pan-sharpened spectral bands. A LR PAN band is simulated in one of the two methods: In the first method, the appropriate LR MS bands are combined into a single, simulated LR PAN by calculating the appropriate weights. In order to combine the MS data (B, G, R and NIR bands) into the simulated PAN band, weights for each of the 4 bands can be calculated by

$$B_{wt} = \int_{0.4}^{0.5} OT_B(\lambda) * SR_B(\lambda) * SR_{PAN}(\lambda) \mathrm{d}\lambda \quad (9)$$

$$G_{wt} = \int_{0.5}^{0.6} OT_G(\lambda) * SR_G(\lambda) * SR_{PAN}(\lambda) \mathrm{d}\lambda \quad (10)$$

$$R_{wt} = \int_{0.6}^{0.7} OT_R(\lambda) * SR_R(\lambda) * SR_{PAN}(\lambda) \mathrm{d}\lambda \quad (11)$$

$$NIR_{wt} = \int_{0.7}^{0.8} OT_{NIR}(\lambda) * SR_{NIR}(\lambda) * SR_{PAN}(\lambda) \mathrm{d}\lambda \quad (12)$$

where OT is the optical transmittance, SR is the spectral response and λ is the wavelength. For more details see [6]. The simulated PAN band is created by

$$PanBand = (B * B_{wi}) + (G * G_{wi}) + (R * R_{wi}) + (NIR * NIR_{wi}) \quad (13)$$

In the second method, LR PAN is produced from the HR PAN band. The HR PAN is blurred (by the appropriate factor), sub-sampled, and interpolated up to the appropriate scale. The simulated LR PAN is now used as the first band of the LR MS data which is to be input into the original MS band to Gram Schmidt (GS) transform.

$$\mathrm{GS}_1(\mathrm{i,j}) = \mathrm{SimulatedPAN(i,j)} \quad (14)$$

where i is the row number and j is the column number, and GS_1 is the first Gram-Schmidt transformed band. GS method orthogonalises the matrix data or bands of an image which removes redundant (correlated) information that is contained in multiple MS bands. If there were perfect correlation between input bands, the final band will contain all zeros. In GS method, the mean of each band is subtracted from each pixel in the band before the orthogonalisation is performed. The T^{th} GS band is constructed from the previous T-1 GS bands using

$$GS_T(i,j) = (B_T(i,j) - \mu_T) - \sum_{l=1}^{T-1} \phi(B_T, GS_l) * GS_l(i,j) \quad (15)$$

where T is the band number being transformed, B is the original band, and μ_T is the mean of the band T given by

$$\mu_T = \frac{\sum_{j=1}^{C}\sum_{i=1}^{R} B_T(i,j)}{C * R} \quad (16)$$

where C is the total number of columns in the image, R is the total number of rows in the image, and $\phi(B_T, GS_l)$ is given by

$$\phi(B_T, GS_I) = \left[\frac{\sigma(B_T, GS_I)}{\sigma(B_T, GS_I)^2}\right] \quad (17)$$

(i.e. covariance between the given GS band and the original band B, divided by the variance of that GS band).

The mean (μ) and standard deviation (σ) of the first GS band and the HR PAN are then calculated.

$$\sigma_T = \sqrt{\frac{\sum_{j=1}^{C}\sum_{i=1}^{R}(B_T(i,j)-\mu_T)}{C*R}} \quad (18)$$

The HR PAN image (P) is then stretched so that its mean digital count (μ_p) and standard deviation (σ_P) match the mean (μ_{GS1}) and standard deviation (σ_{GS1}) of the first GS band which helps to preserve the spectral characteristics of the original MS data.

$$\text{Modified P}=(\text{P}\times\text{Gain})+\text{Bias} \quad (19)$$

where, $Gain = \frac{\sigma_I}{\sigma_P}$ and $Bias = \mu I - (Gain * \mu P)$

The stretched HR PAN band and the first GS band, which is actually the simulated LR PAN band have similar global and local statistics. The stretched HR PAN image is then swapped for the first GS band, and the data is transformed back into original MS space producing HR MS bands by (20).

$$B_T(i,j) = (GS_{T(i,j)} + \mu_T) + \sum_{i=1}^{T-1}\phi(B_T, GS_I) * GS_I(i,j) \quad (20)$$

D. CN Spectral (CNS): CNS sharpening can be used to simultaneously sharpen any number of bands and retains the input image's original data type and dynamic range. Input MS bands are sharpened only if they fall within the spectral range of one of the Sharpening Image's bands (PAN band). The spectral range of the PAN is defined by the band center wavelength and full width-half maximum (FWHM) value, both obtained from the PAN image. MS bands are grouped into spectral segments defined by the spectral range of the PAN band. Each MS band is multiplied by the PAN band, then normalized [7]. For a MS data with 4 bands, the above formula may be generalised as

$$MS_i^H = \frac{4(MS_i^L)\cdot PAN}{(\sum_i MS_i^L)+4} - 1 \quad (21)$$

where MS_i^H are the fused images, MS_i^L are the LR MS bands, PAN is a HR panchromatic band, and i = band 1 to band 4.

E. Luminance Chrominance (LC): YIQ has a straightforward transformation from RGB with no loss of information [8]. Y is the luminance (brightness of a PAN image) which combines the red, green, and blue signals in proportion to the human eye's sensitivity to them, I is red minus cyan and Q is magenta minus green. The relations between YIQ and RGB are (22) and (23):

$$\begin{pmatrix} Y \\ I \\ Q \end{pmatrix} = \begin{pmatrix} 0.299 & 0.587 & 0.114 \\ 0.596 & -0.274 & -0.322 \\ 0.211 & -0.523 & 0.312 \end{pmatrix} \begin{pmatrix} R \\ G \\ B \end{pmatrix} \quad (22)$$

$$\begin{pmatrix} R \\ G \\ B \end{pmatrix} = \begin{pmatrix} 1.000 & 0.996 & 0.621 \\ 1.000 & -0.272 & -0.647 \\ 1.000 & -1.106 & -1.703 \end{pmatrix} \begin{pmatrix} Y \\ I \\ Q \end{pmatrix} \quad (23)$$

F. High pass fusion (HPF): HPF method convolves a high pass filter over a HR image to extract spatial information and a low pass filter over a LR image to extract spectral information. Two images are combined as proposed by Vrabel (1996) [9] given in (24).

$$(W_1 \times LR_i) + (W_2 \times HR). \quad (24)$$

W1 and W2 are weights with W1 + W2 = 1, LRi is the LR band after low pass filtering and HR is the PAN band after high pass filtering. Experimentally, it was determined that the best balance of spectral and spatial information involved weights of W1=0.80, W2=0.20 [10].

III. DATA ANALYSIS AND RESULTS

IKONOS PAN data at 11 bits per pixel (525.8 – 928.5 μm, 1 m resolution, acquired on February 23, 2004) of size 1200 x 1600 and 4 m resolution MS bands (Red, Green, Blue and NIR, acquired on November 24, 2004) of size 300 x 400, covering a portion of Bangalore city, India were used to test the performance of the methods. The pairs of the images were registered to each other and the LR images were upsampled to 1200 x 1600 by nearest neighbour algorithm. The correlation coefficients (CCs) between PAN (downsampled to 4 m pixel size) and the original Blue band was 0.41, PAN and Green was 0.44, PAN and Red was 0.47 and PAN and NIR was 0.59. CC of the NIR band is higher than CCs of other bands, indicating that IKONOS NIR band is very important to the IKONOS PAN band. Fig. 1 (A) shows the PAN image and (B) shows the false colour composite (FCC) of the G-R-NIR combination resampled at 1 m pixel size. It is obvious that PAN image has better spatial resolution than the MS images and more detail can be seen in the PAN image. Image fusion is attempted here to simulate IKONOS MS data acquired at LR (4 m) to HR (1 m), which is identical to MS images had there been a ideal sensor that would originally acquire MS at high resolution (1 m). G-R-NIR combination was chosen for generating FCC in LC method, which can consider only 3 bands. In the ATW method decomposition level (*n*) was set to 2 as the resolution ratio between the IKONOS PAN and MS is 1:4. Low pass and high pass filters of size 3×3 were used in the HPF method. Fig. 1 (C–H) depicts the FCC of the fused images at 1 m obtained from ATW, MRAIM, GS, CNS, LC and HPF methods. The performance is evaluated in terms of the quality of synthesis of both spatial and spectral information. MRAIM and LC (Fig. 1 D and G) produce significant color distortion, while ATW, CNS and HPF (Fig. 1 C, F and H) produce slight colour distortion in buildings/builtup area. ATW, MRAIM, and HPF exhibit sharpness due to enhancement along the edges because these methods have considered the high-frequency information between the PAN and the MS bands. A universal image quality index (UIQI) to measure the similarity between two images [4] is designed by a combination of (i) loss of correlation, (ii) radiometric distortion, and (iii) contrast distortion given by 25.

$$UIQI = \frac{\sigma_{AB}}{\sigma_A \sigma_B} \cdot \frac{2\mu_A\mu_B}{\mu_A^2+\mu_B^2} \cdot \frac{2\sigma_A\sigma_B}{\sigma_A^2+\sigma_B^2} \quad (25)$$

The first component is the CC for A (original MS band)

and B (fused MS band). The second component measures how close the mean gray levels of A and B is, while the third measures the similarity between the contrasts of A and B. The dynamic range is [-1, 1]. If two images are identical, the similarity is maximal and equals 1. The synthesised HR MS images are spatially degraded to the resolution level of the original LR MS images (4 m). UIQI are computed between the degraded HR MS images and the original LR MS images. Table I shows that the UIQI values of the HPF, ATW and MRAIM methods are higher than the UIQIs of other methods. The UIQI of ATW in the NIR band is highest than the other values. Table II shows the CC between the IKONOS HR PAN image and the corresponding simulated LR PAN images by different methods (computed at 1 m pixel size). HPF, ATW and MRAIM show high CC with respect to the corresponding LR PAN image. It can be seen from Tables I and II that the degree of similarity between the HR PAN image and the LR PAN image correspond to the degree of spectral distortion of each band. The lower the similarity between the HR PAN image and the LR PAN image, the higher the spectral distortion and vice versa. Therefore from the UIQI method, HPF is superior to all other methods but only slightly better than ATW. The closeness between two images was quantified in terms of correlation (Fig. 2). Each band of the original IKONOS MS data were correlated with respect to the corresponding fused band obtained from the 6 techniques (except in LC where only G, R, and NIR were considered).

TABLE I.
UIQI MEASUREMENTS OF THE SIMILARITY BETWEEN ORIGINAL AND THE FUSED IMAGES OBTAINED BY VARIOUS METHODS

	Blue	Green	Red	NIR
ATW	0.83	0.92	0.95	0.99
MRAIM	0.81	0.89	0.91	0.93
GS	0.49	0.44	0.46	0.43
CNS	0.12	0.29	0.43	0.43
LC	-	0.12	0.92	0.61
HPF	0.93	0.94	0.93	0.94

TABLE II.
CORRELATION BETWEEN THE IKONOS HR PAN IMAGE AND THE CORRESPONDING LR PAN IMAGE BY DIFFERENT METHODS

ATW	MRAIM	GS	CNS	LC	HPF
0.85	0.80	0.65	-	0.71	0.86
p value for all CC = 2.2e-16					
LC is limited to three bands (G-R-NIR combination). PAN image was used in CNS without any transformation.					

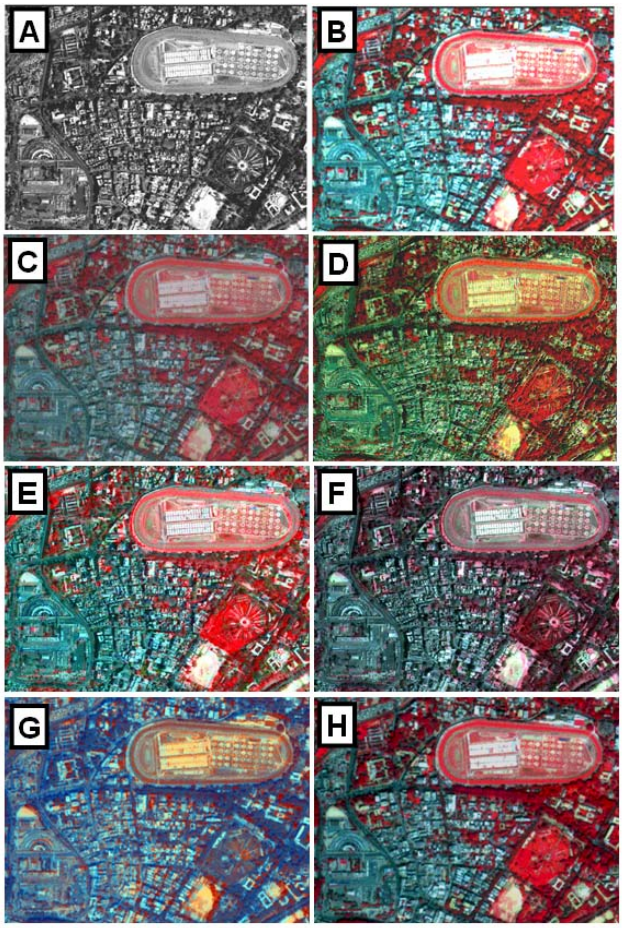

Figure 1. (A) Original PAN image, (B) Original low resolution MS image (G-R-NIR) resampled at 1 m pixel size, fusion results from (C) ATW, (D) MRAIM, (E) GS, (F) CNS, (G) LC and (H) HPF.

HPF followed by ATW and MRAIM produce very high correlation of more than 0.9 with all the bands. Statistical parameters – minimum (min), maximum (max) and the standard deviation (sd) were plotted (Figs. 3–5) to examine the spectral information preservation. HPF and GS were closest to the min values of the original bands, while LC produced negative values. For the max values, in all the bands, values obtained from ATW method were close to the max of original bands. It is to be noted that the max values obtained from one of the best performing method till now – HPF, is lower than the original values for all the 4 bands. GS and CNS were close to original in band 1, 2 and 3 and LC maximum values were close in band 2 and 3 (it does not have band 1 as in other methods). The sd values for the ATW followed by HPF were similar to the original bands of the IKONOS. All other methods showed deviations. ATW and HPF are better compared to other methods. ATW has high UIQI values for Red and NIR bands whereas HPF has highest UIQI scores in Blue and Green bands. The CC values between the HR PAN and LR PAN for ATW is 0.85 and HPF is 0.86. The CC between fused and original band is higher for HPF method and the min values of the fused images from HPF are also closest to the original PAN image. However, the max values and the sd values of the fused bands obtained from ATW are closest to the original band values.

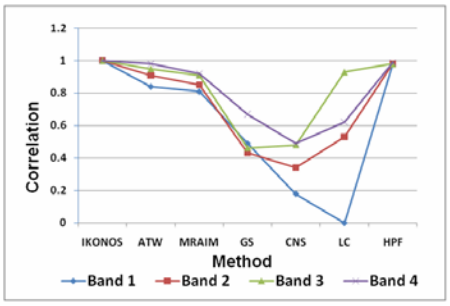

Figure 2. Correlation between original images and corresponding fused images.

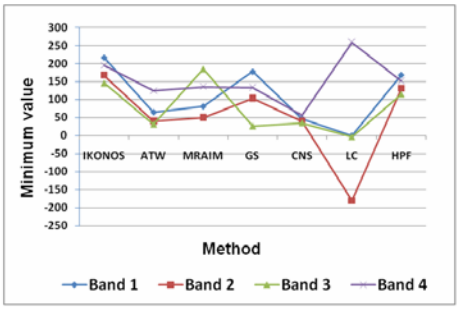

Figure 3. Minimum values of the original images and the fused images.

This give an ambiguous result as both methods have very much similar scores and the results remain inconclusive. Hence, the only measure that can decide the best technique among the two is the role of the NIR band in these methods for which the CC was found highest with PAN band (0.59). Fused NIR band obtained from ATW (table III) is close to original NIR band in terms of UIQI, max value and sd values whereas HPF method results is closest to original NIR band in terms of CC and min values. Overall ATW has a lead in terms of UIQI measure, so we conclude that ATW method followed by HPF produce the images closest to those the corresponding multisensors would observe at the HR level.

IV. Conclusion

ATW followed by HPF are best among the six techniques discussed here for image fusion as the output is closest to what is expected had there been a corresponding multisensor observation at the high resolution level of PAN.

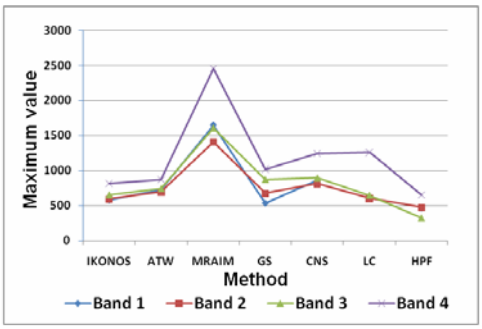

Figure 4. Maximum values of the original images and the fused images.

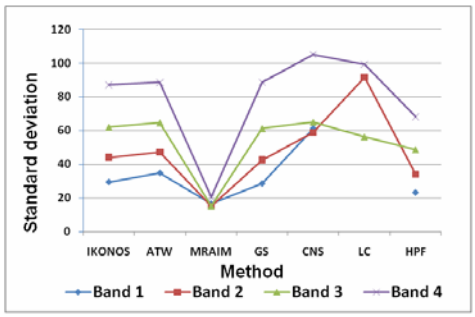

Figure 5. Standard deviation of the original and the fused images.

TABLE III.
EVALUATION OF ORIGINAL AND FUSED NIR BAND BY DIFFERENT METHODS

	UIQI	CC	Min	Max	Sd
Original NIR	1	1	195	811	87
Fused NIR (ATW)	**0.99**	0.98	125	**867**	**88.5**
Fused NIR (HPF)	0.94	**0.99**	**152**	650	68.1

Acknowledgment

We extend our sincere thanks to GeoEye Foundation, USA for providing us the high resolution IKONOS imagery of Greater Bangalore without which research results would have been difficult to validate. We are also grateful to Indian Institute of Science, Bangalore for financial and infrastructure support.

References

[1] J. Nunez, X. Otazu, O. Fors, A. Prades, V. Pala, and R. Arbiol, "Multiresolution-Based Image Fusion with Additive Wavelet Decomposition," *IEEE Transactions of Geoscience and Remote Sensing*, vol. 37(3), pp. 1204-1221, 1999.

[2] J. L. Starck and F. Murtagh, "Image restoration with noise suppression using the wavelet transform," *Astron. Astrophys*, vol. 228, pp. 342-350, 1994.

[3] Z. Wang, D. Ziou, C. Armenakis, D. Li, and Q. Li, "A Comparative Analysis of Image Fusion Methods," *IEEE Transactions of Geoscience and Remote Sensing*, vol. 43 (6), pp. 1391-1402, 2005.

[4] P. Steffen, P. Heller, R. A. Gopinath, and C. S. Burrus, "Theory of regular M-band wavelet Bases," 1993. URL: http://www.supelec-rennes.fr/ren/perso/jweiss/wavelets.html

[5] M. J. Shensa, "The discrete wavelet transform: wedding the À Trous and Mallat algorithms," *IEEE transactions on Signal Processing*, vol. 40 (10), pp. 2464-2482, 1992.

[6] C. A. Laben, and B. V. Brower, "Process for enhancing the spatial resolution of multispectral imagery using pan-sharpening," United States Eastman Kodak Company (Rochester, NY). US Patent 6011875, 2000. URL: http://www.freepatentsonline.com/6011875.html.

[7] J. Vrabel, P. Doraiswamy, J. McMurtrey and A. Stern, "Demonstration of the Accuracy of Improved Resolution Hyperspectral Imagery," *SPIE Symposium Proceedings*, 2002.

[8] C. Pohl and J. L. Van Genderen, "Multisensor image fusion in remote sensing: concepts, methods and applications**,"** *International Journal of Remote Sensing*, vol. 19(5), pp. 823- 854, 1998.

[9] J. Vrabel, "Multispectral Imagery Band Sharpening Study." *Photogrammetric Engineering and Remote Sensing*, 62(9), pp. 1075-1083, 1996.

[10] *Analysis of Fusion Techniques for Forestry Applications*, Highland Geographic Incorporated, State University of New York College of Environmental Science and Forestry Affiliated Research Center submitted to NASA Commercial Remote Sensing Program Office, John C. Stennis Space Center, MS 39529, 1999.